Carbon 228 (2024) 119384

Contents lists available at ScienceDirect

Carbon

journal homepage: www.elsevier.com/locate/carbon

Easy functionalization of carbon nano-onions with disulfides and their use as recyclable heterogeneous organocatalysts

Alessandro Mercadante [a], Michal Bartkowski [b], Vincenzo Campisciano [a], Valeria La Parola [c], Alberto Spinella [d], Raul Arenal [e,f,g], Michelangelo Gruttadauria [a], Silvia Giordani [b,**], Francesco Giacalone [a,*]

[a] Department of Biological, Chemical and Pharmaceutical Sciences and Technologies, University of Palermo and INSTM UdR Palermo, Viale delle Scienze, Ed. 17 90128, Palermo, Italy
[b] School of Chemical Sciences, Dublin City University, Glasnevin, Dublin 9, Ireland
[c] Institute for the Study of Nanostructured Materials, National Research Council (ISMN -CNR), Via Ugo La Malfa 153, 90146, Palermo, Italy
[d] Advanced Technologies Network Center (ATeN Center), University of Palermo, via F. Marini 14, 90128, Palermo, Italy
[e] Instituto de Nanociencia y Materiales de Aragon (INMA), CSIC-U. de Zaragoza, 50009, Zaragoza, Spain
[f] Laboratorio de Microscopias Avanzadas (LMA), Universidad de Zaragoza, 50018, Zaragoza, Spain
[g] ARAID Foundation, 50018, Zaragoza, Spain

ARTICLE INFO

Keywords:
Carbon nano-onions
PAMAM dendrimers
Heterogeneous catalysis
2-Amino-4H-chromene derivatives
Three-component one-pot synthesis

ABSTRACT

A facile functionalization of carbon nano-onions (CNO), through an atom economical one-step process, with a series of different generation (2.0, 2.5, and 3.0G) poly(amidoamine) (PAMAM) dendrimers with a cystamine core and endowed with either methyl ester or amino groups in the periphery has been reported. The radical addition reaction onto CNO surface, after the homolytic rupture of the S–S bond of cystamine, afforded CNO-PAMAM hybrids, which were extensively characterized using various analytical and spectroscopic techniques such as thermogravimetric analysis (TGA), attenuated total reflectance-Fourier transform infrared (ATR-FTIR) spectroscopy, solid state ^{13}C NMR, Raman, X-ray photoelectron spectroscopy (XPS), dynamic light scattering (DLS) and zeta potential (ZP). Morphological and textural properties were also investigated by high-resolution transmission electron microscopy (HRTEM) analysis and N_2 adsorption/desorption isotherms. Furthermore, the presence and availability of $–NH_2$ groups has been demonstrated by applying the functionalized CNO with PAMAM 2.0G and 3.0G as heterogeneous and recyclable organocatalysts in the one-pot three-component synthesis of 2-amino-4*H*-chromene derivatives.

1. Introduction

The ability of carbon to exist in several nanoallotropic forms comprising 0D, 1D, and 2D structures organized in strings, tubes, sheets, spheres, or multi-layered spheres (nano-onions), has attracted tremendous interest from the scientific community due to their potential use in several applications, mainly in the field of nanotechnology [1–5]. Despite their outstanding mechanical, physical, and electronic properties, carbon nanomaterials (CNMs) usually display poor solubility and bad dispersibility in common solvents that strongly hampers their wider use, limiting their potential.

Carbon nano-onions (CNO) structurally consist of multiple concentric fullerene-like shells. As is typical for a member of the CNM family, CNO show aggregation due to the strong intermolecular electrostatic interactions, dominated by van der Waal forces, established through their large external surface area.

To overcome the poor dispersibility of CNO, their surface chemical functionalization may represent a double solution; on the one hand, preventing their aggregation and, on the other, allowing to obtain new materials that combine CNO' intrinsic properties with those of the functionalizing moieties [6]. In this regard, protocols [7] have been adopted for covalent modification of CNO: besides the classic oxidation and amidation strategy, which deeply alter the CNO-surface [8,9], other chemical functionalization includes fluorination [6], [2 + 1]

* Corresponding author.
** Corresponding author.
E-mail addresses: silvia.giordani@dcu.ie (S. Giordani), francesco.giacalone@unipa.it (F. Giacalone).

https://doi.org/10.1016/j.carbon.2024.119384
Received 22 March 2024; Received in revised form 4 June 2024; Accepted 22 June 2024
Available online 24 June 2024

cycloaddition of nitrenes [10], Prato reaction [9,11], Tour reaction [12,13] and more recently the Birch reaction [14,15].

As stated, the chemical derivatization of CNO along with the possibility for their gram-scale synthesis has allowed to use the functionalized materials for several applications such as energy and electrochemical storage [16,17], sensing [18–20], supercapacitors [21,22], fuel cells [23] and water treatment [24].

Significantly, the versatility [25] of CNO has given way to their biomedical applications [26]. Their biocompatibility and easy penetration into cells, demonstrated through their use in bioimaging [27,28], their efficient delivery of glycopeptides and proteins [29], and their targeted delivery of anticancer therapeutics [30], underline their capacity as non-cytotoxic carriers for cellular uptake [31].

The use of CNO as catalysts has been less explored despite their promising roots in the oxidative dehydrogenation of ethylbenzene [32,33]. Pristine or oxidized CNO were employed as nanocomposites with Bi_2O_3 or NiCu nanoparticles for the photocatalytic thiol-ene reaction [34] or C–C coupling processes [35], respectively. Furthermore, the graphitic shells of CNO were used to trap Pt single atoms and used for the hydrogenation of nitroarenes [36], whereas CNO structures were modified with iron oxide to be applied as photocatalysts for degradation of persistent pollutants [37]. Nitrogen-rich CNO [38] and nitrogen-doped CNO hybrids with molybdenum carbide [39] or heteropoly acid [40] have been, in turn, used as heterogeneous catalysts for the oxygen reduction reaction, and alkene dehydrogenation and ester hydrolysis reactions, respectively. Recently, a series of CNO-metallophthalocyanine conjugates have been applied as photocatalysts for degrading rhodamine B [41].

However, except for the recent case, the above studies deal only with unfunctionalized or oxidized CNO. In this regard, we believe CNO represent a viable scaffold for developing recyclable heterogeneous catalysts.

Nevertheless, new versatile and reliable methods for the covalent functionalization of CNO as chemical tools for their easy manipulation are always welcome, especially those avoiding harsh conditions that may alter the electronic properties, since they allow accede to novel hybrid advanced functional materials.

Herein, we report the facile functionalization of CNO, through an atom economical one-step process, with a series of poly(amidoamine) (PAMAM) dendrimers endowed with either methyl ester or amino groups in the periphery, and a cystamine core of varying generation.

The presence and availability of $–NH_2$ groups, in the case of the full-generation dendrimers (2.0G or 3.0G), make them interesting systems that can be exploited for catalytic purposes. Among their possible applications, we chose to test these hybrids as heterogeneous and recyclable organocatalysts in the one-pot three-component synthesis of 2-amino-4*H*-chromene derivatives, which represent vital compounds because of their widespread presence in nature and biological activity [42]. Furthermore, 2-amino-4*H*-chromene derivatives find therapeutic applications in medicinal chemistry as anti-HIV, anti-tumor, anti-inflammatory, antifungal, antimicrobial, and anti-allergenic [43–46] among others.

2. Materials and methods

Chemicals and solvents were purchased from commercial suppliers and used as received without further purification. Cystamine-core PAMAM dendrimers were prepared according to the reported literature procedures [47,48].

Thermogravimetric analysis (TGA) was performed under nitrogen flow from 100 to 1000 °C with a heating rate of 10 °C min^{-1} with a Mettler Toledo TGA/DSC STAR System. The temperature was increased starting from RT up to 100 °C, and then this temperature was kept for 30 min to remove adsorbed water or volatile solvents before reaching 1000 °C.

^{13}C Cross-Polarization Magic Angle Spinning (CP-MAS) NMR spectra were acquired on a Bruker Advance II 400 spectrometer operating at 100.63 MHz for ^{13}C nuclides and 400.15 MHz for ^{1}H nuclides equipped with a 4 mm (H–X) double channel CPMAS probe. The samples were placed in a 4 mm zirconia rotor closed with Kel-F caps. The spectra were measured as 1024 scans at a MAS speed of 8 kHz, with 2 ms contact time, 3 s delay time, and an excitation pulse of 4.7 ms on the ^{1}H nucleus. The Hartmann–Hahn condition was optimized using an adamantane standard sample, which was also used as an external chemical shift reference.

ATR-FTIR spectra were recorded on a Thermo Scientific Nicolet Summit Spectrometer with an Everest Diamond ATR accessory over the range of 4000-500 cm^{-1}. The resolution was set to 4 cm^{-1} and the velocity of the mirror was set to 0.4747 cm/s, with background measurement was performed for every sample. The spectra of functionalized CNO were taken at 128 scans to improve S/N ratio, with all other samples taken at 32 scans. Detection was carried out by a DTGS KBr detector with the aperture set to large (100). Prior to FT, apodization was done using the Norton Beer Strong method to mitigate truncation errors. A zero-filling factor of 2 was used to avoid clipping of spectral bands, and automatic atmospheric suppression was enabled.

Raman spectra were acquired using Horiba LabRam HR Evolution equipment with a 532 nm laser line, using laser power reduced to 5 % of its nominal value (70 mW) to avoid sample degradation or heating during the measurements. All Raman spectra represent an average of n = 3 scans, with **CNO-PAMAM 2.5G** representing n = 5 scans. Background correction has been carried out for each material. Baseline correction was carried out using cubic spline interpolation. Smoothing was performed using the Savitzky-Golay filter with a window size of 7 and polynomial order of 3, and the p = 0.05 confidence band has been fitted. Deconvolution was achieved by applying a Lorentzian fit to the D, G, 2D and D + G bands. The I_D/I_G and I_{2D}/I_G ratios were calculated from the intensity integral of the deconvoluted bands. The standard deviation of the I_D/I_G and I_{2D}/I_G ratios was calculated by fitting each individual spectrum and introducing randomized shifts to the baseline cubic spline interpolation anchor points (up to a maximum of 10 cm^{-1}), for a sample size of n = 96 for each ratio. To assess whether the I_D/I_G and I_{2D}/I_G ratios of the CNO-PAMAM xG materials differ significantly from those of p-CNOs, a one-way ANOVA with post-hoc Tukey's test was carried out, and the representative statistics (*$p < 0.05$; **$p < 0.01$; ***$p < 0.001$) were shown.

X-ray photoelectron spectroscopy (XPS) analyses were performed with a VGMicrotech ESCA 3000Multilab, equipped with a dual Mg/Al anode. The spectra were excited with the unmonochromatized Al Kα source (1486.6 eV) run at 14 kV and 15 mA. The analyzer was operated in the constant analyzer energy mode. A pass energy of 20 eV set across the hemispheres was used for the individual peak energy regions. Survey spectra were measured at 50 eV pass energy. The sample powders were mounted on a double-sided adhesive tape. The pressure in the analysis chamber was in the range of 10^{-8} Torr during data collection. The constant charging of the samples was removed by referencing all the energies to the C1*s* set at 284.6 eV. The invariance of the peak shapes and widths at the beginning and end of the analyses ensured the absence of differential charging. Analyses of the peaks were carried out with the software provided by VG, based on the non-linear least-squares fitting program using a weighted sum of Lorentzian and Gaussian component curves after background subtraction, according to Shirley and Sherwood [49]. Atomic concentrations were calculated from peak intensity using the sensitivity factors provided by the software. The binding energy values are quoted with a precision of ±0.15 eV, and the atomic percentage with a precision of ±10 %.

High-resolution transmission electron microscopy (HRTEM) has been performed using a Tecnai F30 microscope (FEI-Thermo Fisher Scientific, Eindhoven, The Netherland) working at 300kV. The HRTEM samples were prepared by dispersing a drop of the ultrasonicated suspension in ethanol onto carbon holey-supported Cu grids.

The textural properties were obtained by N_2 adsorption/desorption

isotherms using Micromeritics ASAP2020 Plus 1.03 (Micromeritics, Norcross, GA 30093, USA). Before the analyses, samples were outgassed at 100 °C for 4 h to clean the surface and make also the pores available for N_2 adsorption. The fully computerized analysis of the N_2 adsorption isotherm at - 196 °C in the standard pressure range 0.05–0.3 p/p0 allowed us to obtain, through Brunauer–Emmett–Teller (BET) model, the specific surface areas (SSA) of the samples. The micropore presence was evaluated using the t-plot method. The total pore volume (Vp) and pore size distribution (dV/dw) were evaluated by applying the Barrett–Joyner–Halenda (BJH) model to the desorption branch of isotherms.

Dynamic light scattering (DLS) and zeta potential (ZP) studies were carried out on CNO functionalized with three generations of PAMAM; namely, **CNO-PAMAM 2.0G**, **CNO-PAMAM 2.5G**, and **CNO-PAMAM 3.0G**. Each material was analyzed at 5, 10 and 20 ppm; briefly, all samples were dispersed in deionized H_2O and sonicated for 15 min prior to analysis. The sonic-bath temperature was maintained at 22–26 °C, and samples were equilibrated to 25 °C prior to DLS, and subsequent ZP, analysis. The analyses were carried out on a ZetaSizer Ultra instrument in backscatter mode, using a PCS1115 cell for DLS measurements and a DTS1070 cell for ZP measurements. Each sample was analyzed 3–6 times each by DLS and ZP, with measurements carried out in 5 min intervals. ZS XPLORER software was used for instrument control, data acquisition and statistical analysis. All standard deviations are calculated from multiple ($n \geq 3$) experiments, and mean diameters are reported from the highest intensity peaks. Data was plotted using a custom python script utilizing the matplotlib package. The DLS temporal analysis plot represents the weighed mean diameter by intensity ordered by area plotted as a function of time from the acquisition of the first measurement post sample preparation. Statistical analysis, including the standard error of the slope in linear regression and the regression fitting of the 95 % confidence band, were carried out in python using the scipy.stats package.

2.1. Preparation of p-CNOs

Detonation nanodiamonds (DNDs) were purchased from Carbodeon Ltd. (uDiamond® Molto; 4–6 nm particle diameter). Briefly, pristine carbon nano-onions (p-CNOs), measuring 6–7 nm in diameter with 6–8 concentric shells, were synthesized by thermally annealing DNDs at 1650 °C in a tube furnace under a helium atmosphere, as per a patented protocol [50].

2.2. Preparation of CNO-PAMAM 2.0G

In a 50 mL flask, 15 mg of pristine CNO (p-CNO) (1.25 mmol) were suspended in 10 mL of toluene and sonicated for 15 min. A solution of 1.0 g PAMAM 2.0G (0.66 mmol) in 4 mL of methanol was added to the p-CNO suspension and degassed for 15 min. Then, 25 mg of azobisisobutyronitrile (AIBN) (0.15 mmol) were added and the mixture was heated at 100 °C for the indicated time under Ar atmosphere. The resulting dispersion was allowed to cool, filtered on a Millipore membrane (PTFE 0.45 μm) and the residue was washed with toluene, MeOH, water, 3.0 M HCl, 2 % v/v triethylamine in THF, THF and diethyl ether. The resulting black solid was dried under vacuum at 40 °C overnight.

2.3. Preparation of CNO-PAMAM 2.5G(I and II)

In a 50 mL flask 15 mg of p-CNO (1.25 mmol) were suspended in 8 mL of toluene and sonicated for 15 min. A solution of 1.0 g PAMAM 2.5G (0.35 mmol) in 2 mL of methanol was added to the p-CNO suspension and the mixture was heated at 100 °C for 72 h, in the case of **CNO-PAMAM 2.5G(I)**, or 96 h, in the case of **CNO-PAMAM 2.5G(II)**. The resulting dispersion was allowed to cool, filtered on a Millipore membrane (PTFE 0.45 μm), and the residue was washed with toluene, MeOH, and diethyl ether. The resulting black solid was dried under vacuum at 40 °C overnight.

2.4. Preparation of CNO-PAMAM 3.0G(I and II)

In a 50 mL flask 15 mg of p-CNO (1.25 mmol) were suspended in 10 mL of toluene and sonicated for 15 min. A solution of 1.0 g PAMAM 3.0G (0.30 mmol) in 4 mL of methanol was added to the p-CNO suspension and degassed for 15 min. Then, 25 mg of AIBN (0.15 mmol) were added and the mixture was heated at 100 °C for 96 h, in the case of **CNO-PAMAM 3.0G(I)**, or 120 h, in the case of **CNO-PAMAM 3.0G(II)**, under Ar atmosphere. The resulting dispersion was allowed to cool, filtered on a Millipore membrane (PTFE 0.45 μm) and the residue was washed with toluene, MeOH, water, 3.0 M HCl, 2 % v/v triethylamine in THF, THF, and diethyl ether. The resulting black solid was dried under vacuum at 40 °C overnight.

2.5. Synthesis of 2-amino-3-cyano-4-(4-bromophenyl)-4H-benzo[h]chromene (1)

In a 5 mL glass vial with screw cap, 1-naphthol (0.2 mmol), malononitrile (0.2 mmol), 4-bromobenzaldehyde (0.2 mmol), and the catalyst (6 mg; ~3 mol% for **CNO-PAMAM 2.0G**; ~12 mol% for **CNO-PAMAM 3.0G(II)**) were introduced and 0.5 mL deionized water was added. The reaction mixture was shortly sonicated to disperse catalyst and stirred at 70 °C for 2 h. The reaction mixture was allowed to cool down to room temperature. Afterwards, acetone was added before sonication to dissolve all the reactants/product and recover the catalyst by centrifugation. The washings with acetone were repeated twice and all supernatants were combined, dried under reduced pressure, and analyzed by ^{1}H NMR spectroscopy. The recovered catalyst was dried at 60 °C before being reused in the next cycle.

2.6. Synthesis of 2-amino-4-(3-bromophenyl)-7,7-dimethyl-5-oxo-5,6,7,8-tetrahydro-4H-chromene-3-carbonitrile (2)

In a 5 mL glass vial with screw cap, dimedone (0.25 mmol), malononitrile (0.3 mmol), 4-bromobenzaldehyde (0.25 mmol), and the catalyst (2 mg, ~3 mol% of **CNO-PAMAM 3.0G(II)**) were introduced and 0.5 mL deionized water was added. The reaction mixture was shortly sonicated to disperse catalyst and stirred at 90 °C for 1 h. The work up procedure was the same as described above.

3. Results and discussion

The hybrids **CNO−PAMAM 2.0G**, **2.5G**, and **3.0G** (Scheme 1) have been prepared through the atom-economical strategy which involves the direct reaction of p-CNO with disulfides—namely, PAMAM dendrimers with *x*G cystamine core, where *x* is generation 2.0, 2.5 or 3.0—through a toluene-reflux protocol developed for other carbon nanoforms [51–53]. The full-generation dendrimer (2.0G or 3.0G) is comprised of two or three layers of branching points and has amino groups at the ends, whereas the middle generation (2.5G) indicated two layers and the presence of methyl ester group at the ends. PAMAM dendrimers have found application as macromolecular vectors for drug delivery [54–57] as well as in biomedical applications [58–60], and the presence of $–NH_2$ groups and methyl esters in the periphery allows for their possible post-functionalization through amidation, nucleophilic substitution or formation of carbamates for the former, and hydrolysis and esterification for the latter. To functionalize CNO with the full generation PAMAM dendrimers (2.0G and 3.0G), AIBN was utilized, as per analogous reactions between thiols and several other carbon nanomaterials (CNMs) [61–63].

The reactions were initially kept for four days for the full generation PAMAM (2.0G and 3.0G) and three days for PAMAM 2.5G (Table 1, entries 1–3), but more functionalized materials were obtained when the reaction with PAMAM 2.5G and 3.0G were maintained one day longer

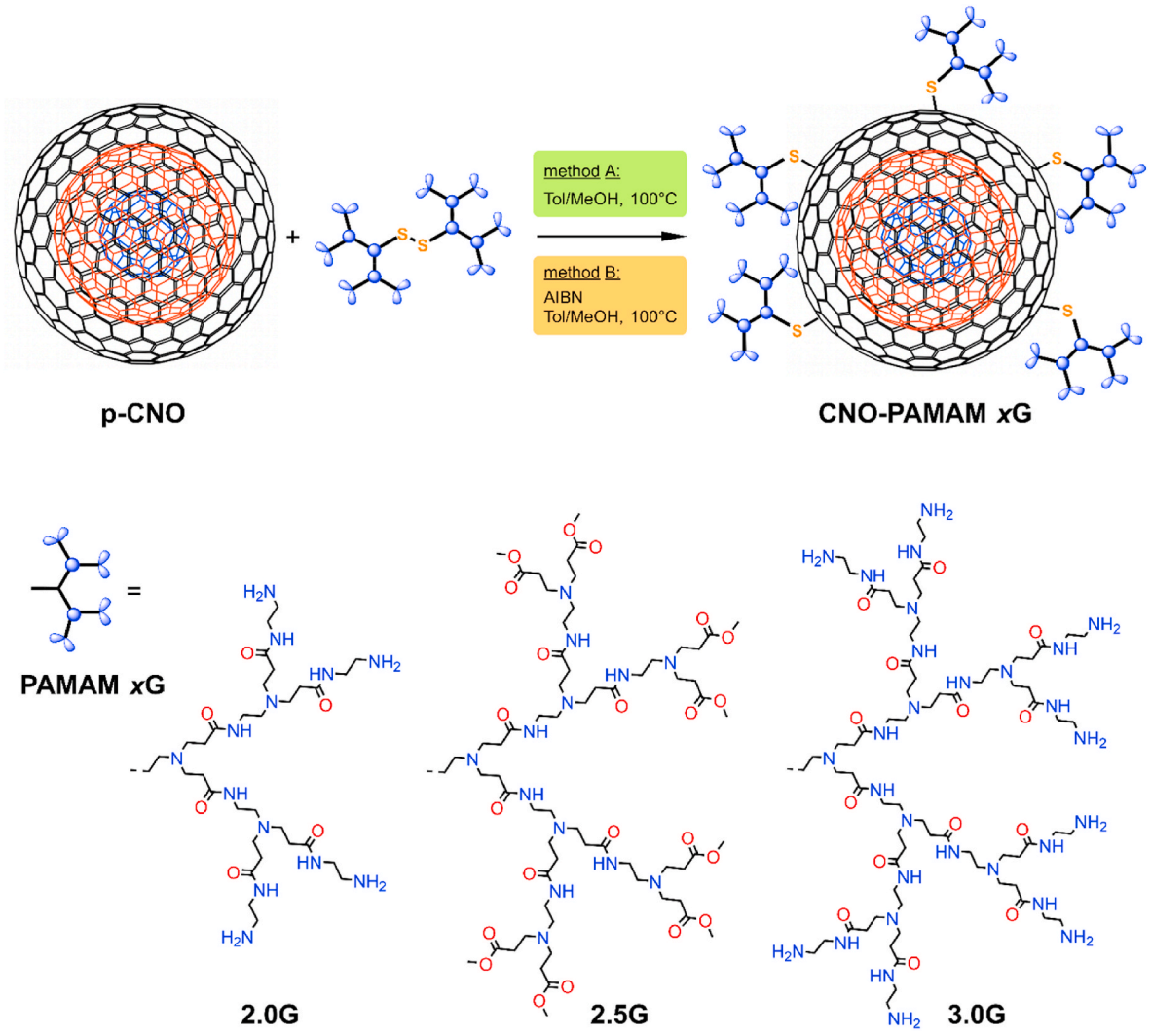

Scheme 1. Synthesis of CNO-PAMAM *x*G hybrids from p-CNO through methods A and B, and the structure of the corresponding PAMAM generations.

Table 1
Preparation of CNO-PAMAM hybrids and loading in PAMAM dendrons and amino groups.[a]

Entry	Material	Method	Solvent ratio (total volume)	Time (h)	Loading (mmol/g)[b]	-NH_2 content (mmol/g)
1	CNO-PAMAM 2.0G	B	MeOH:Tol 2:5 (14 mL)	96	0.235	0.94
2	CNO-PAMAM 2.5G(I)	A	MeOH:Tol 1:4 (10 mL)	72	0.149	–
3	CNO-PAMAM 3.0G(I)	B	MeOH:Tol 2:5 (14 mL)	96	0.152	1.22
4	CNO-PAMAM 2.5G(II)	A	MeOH:Tol 1:4 (20 mL)	96	0.511	–
5	CNO-PAMAM 3.0G(II)	B	MeOH:Tol 2:5 (14 mL)	120	0.526	4.21

[a] Reaction conditions: Method A – 15 mg of CNO, 1 g of PAMAM *x*G in methanol/toluene mixture at 100 °C; method B – 15 mg of CNO, 1 g of PAMAM *x*G, 25 mg of AIBN in methanol/toluene mixture at 100 °C.
[b] Determined by TGA at 700 °C.

(Table 1, entries 4–5; see Materials and Methods for conditions). For clarity, the reactions of entries 2 and 3 were left over the weekend, and in both cases, most of the dendrimer adhered to the flask walls above the solvent level. In the repeated reactions, we took care to push, each day of reaction, the dendrimer below the solvent level to be in contact with the solvent and stirred. It is worth mentioning that the title process is 100 % atom economical since all the atoms are linked to the CNO, and the cystamine-cored PAMAM that did not react can be readily recovered by filtration at the end of the process.

Materials **CNO-PAMAM 2.0G**, **CNO-PAMAM 2.5G(I and II)**, and **CNO-PAMAM 3.0G(I and II)**, as well as the parental p-CNO and the three PAMAM generations, were subjected to thermogravimetric analysis (TGA) under nitrogen flow to study both their thermal stability and the functionalization degree of p-CNO. The TGA curves and derivative thermogravimetry (DTG) curves have been presented in Fig. 1, wherein the relevant wt% values have also been outlined. Given that no decomposition of p-CNO was observed up to 700 °C, these wt% values were quantified at 700 °C, ensuring that all organic coatings were decomposed. Further estimation of the functionalization degree of the hybrids has been carried out to assess their PAMAM and peripheral amino content; these values are reported in Table 1.

For **CNO-PAMAM 2.0G**, a net weight loss at 700 °C of 15.8 % can be observed. Moreover, since the parent dendrimer 2.0G showed an 88.3 % decomposition degree (Fig. 1a, red line), this value was used to correct the loading of the dendron corresponding to 17.9 wt%, namely 0.235 mmol/g. Finally, taking into account that the dendron arising from

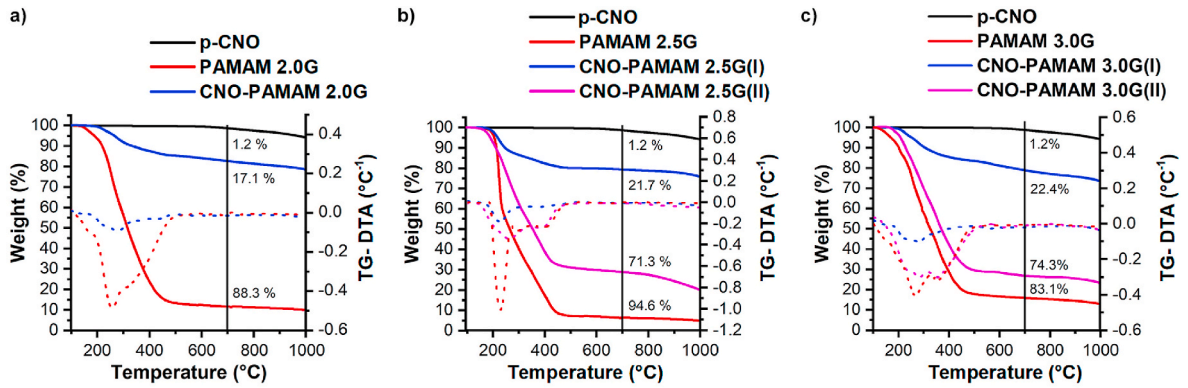

Fig. 1. TGA (solid) and DTG (dashed) curves of p-CNO, PAMAM *x*G dendrimers, and the CNO-PAMAM *x*G hybrids.

PAMAM 2.0G possesses four peripheral amino groups, the NH_2 content was found to be 0.94 mmol/g. In addition, the PAMAM-modified CNO show increased thermal stability compared to their parental PAMAM. **CNO-PAMAM 2.5G(I)** and **CNO-PAMAM 2.5G(II)** show similar thermal behavior with a net weight loss of 20.5 wt% and 70.1 wt%, respectively (Fig. 1b). This indicates that the reaction time can impart control over the degree of functionalization. TGA of **CNO-PAMAM 3.0G(I)** and **CNO-PAMAM 3.0G(II)** indicates that both hybrids are stable somewhat beyond 200 °C showing a net weight loss of 21.2 % and 73.2 %, respectively, which, in accordance with the procedure described above, correspond to 1.22 and 4.21 mmol/g of amino groups (Fig. 1c).

The attenuated total reflectance-Fourier transform infrared ATR-FTIR spectra of all the prepared materials and those of the dendrimers used for their functionalization are reported in Fig. 2. As expected, in the spectra of **CNO-PAMAM 2.0G** and **CNO-PAMAM 3.0G(I)**, we find the presence of two signals at ~1640 and ~1540 cm^{-1} due to the stretching of the amide C═O and the bending of the amide N–H group, respectively, and, in the 3500-3200 cm^{-1} range weak signals are found due to the presence of amino groups. Unique to the spectra of the half-generation dendrimer, which contains ester terminal groups, is the presence of the single bond C–O stretching vibration at ~1210 cm^{-1} and the presence of an additional ester C═O band at ~1740 cm^{-1}. Comparatively, the intensity of the C–N band at ~1030 cm^{-1} is observed to increase with increasing PAMAM generation, which corresponds to the increase in internal tertiary amines.

For the first time, it was possible to obtain solid-state ^{13}C NMR spectra of functionalized-CNO by using the "Cross-Polarization Magic Angle Spinning" technique (CP-MAS ^{13}C NMR) for **CNO-PAMAM 2.5G (II)** and for **CNO-PAMAM 3.0G(II)** (Fig. 3).

The ^{13}C NMR spectrum of **CNO-PAMAM 2.5G** (Fig. 3a) shows a broad signal consisting of two peaks centered at about 35 and 50 ppm. The first corresponds to carbon atoms in α to the amide nitrogen and to the $–CH_2–$ in α to the carbonyl, and the second to the carbon atoms in α to the tertiary amino nitrogen and to the methoxy groups. A well-defined peak at 175 ppm is also observed, which belongs to the carbonyl groups of PAMAM, fully confirming the proposed structure.

The spectrum of **CNO-PAMAM 3.0G(II)** is represented in Fig. 3b and, as in the previous case, it is possible to observe the peak at 174 ppm due to the carbonyl carbon atoms. The aliphatic region appears as a single large and complex signal between 20 and 60 ppm. This is due to the presence of numerous peripheral methylenes of ethylenediamine, which populate the area between 37 and 42 ppm. Again, the spectrum is in excellent agreement with the proposed structure, confirming the successful covalent functionalization of the CNO. For the sake of completeness, it must be mentioned that the characteristic peak at ca. 120 ppm due to the presence of the C(sp^2) framework of CNO structure [64], whose intensity is significantly lowered because of the use of CP-MAS technique, is covered by a spinning sideband of the signal at 175 ppm.

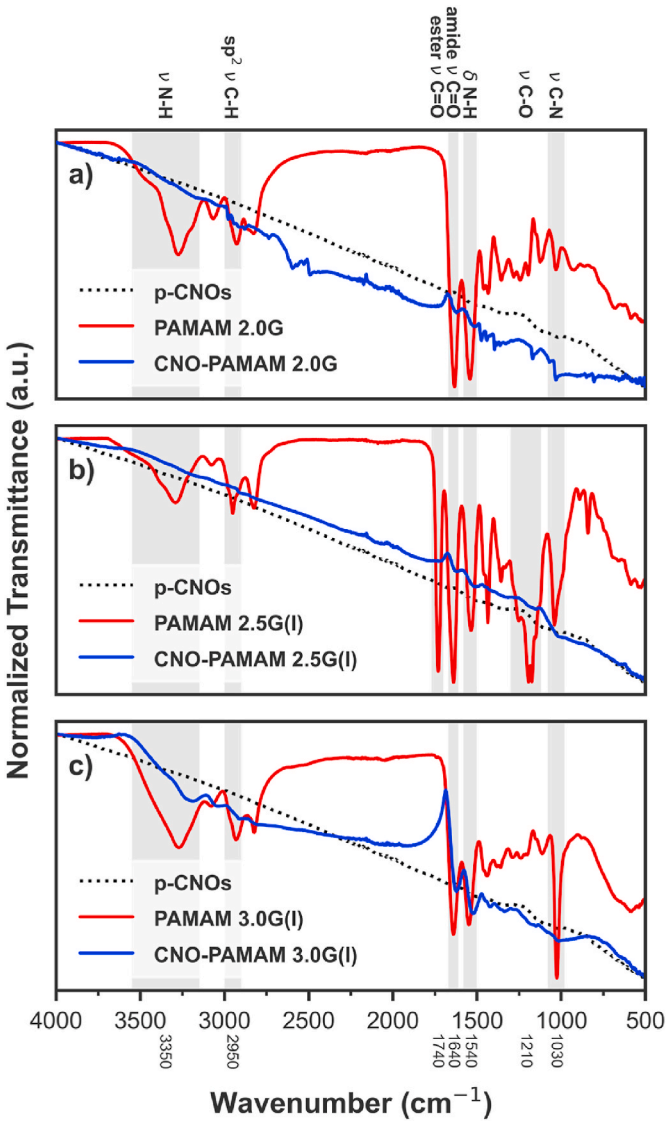

Fig. 2. ATR-FTIR spectra of p-CNO (*dashed*), the three generations of the PAMAM dendrimer and the CNO-PAMAM *x*G hybrids (*solid*). Characteristic peaks have been labeled, where ν signifies stretching vibrations and δ signifies bending vibrations.

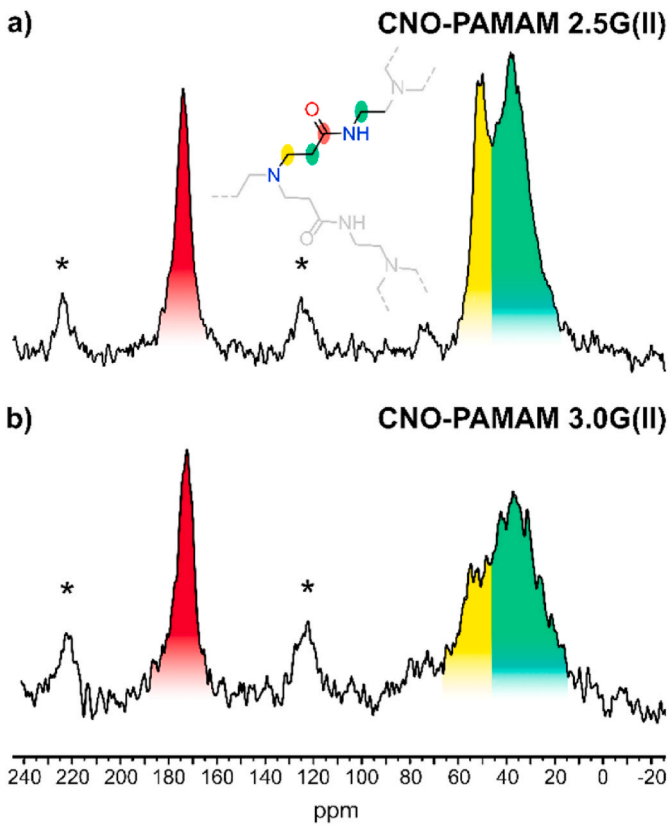

Fig. 3. Solid-state ^{13}C NMR spectra of (a) CNO-PAMAM 2.5G(II); and (b) CNO-PAMAM 3.0G(II) hybrids. Asterisks indicate sidebands.

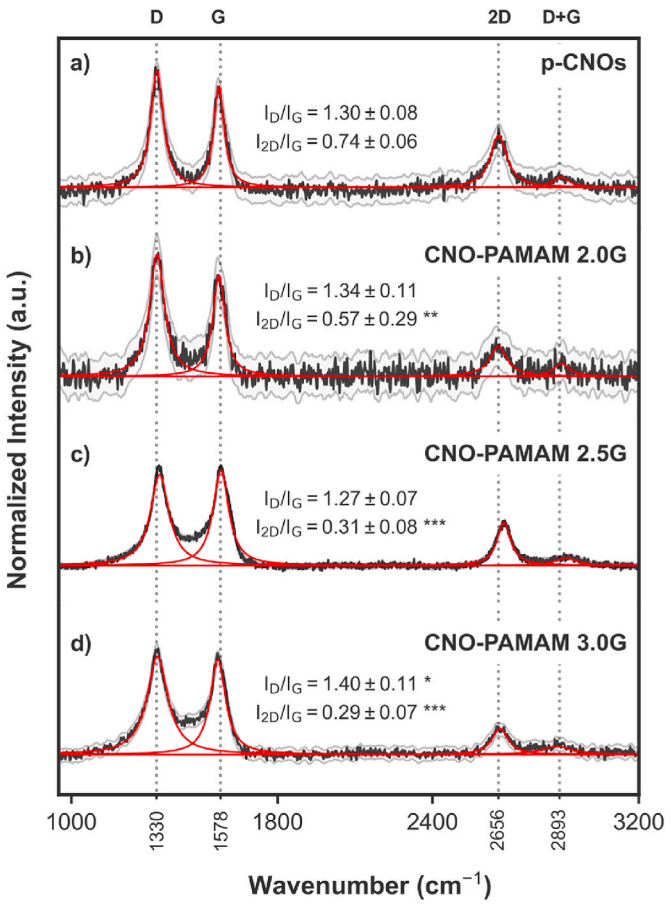

Fig. 4. Raman spectra of p-CNO and the three CNO-PAMAM *x*G hybrids. The spectra (*black*) represent a smoothed average of $n > 3$ scans, with a 95 % confidence band shown (*gray*). The I_D/I_G and I_{2D}/I_G ratios were calculated from the intensity integral of deconvoluted bands (*red*). Statistical significance *vs* p-CNOs has been highlighted, where *p < 0.05; **p < 0.01; ***p < 0.001.

Raman spectroscopy was carried out on p-CNO and the three CNO-PAMAM *x*G hybrids. The spectra, as well as the calculated I_D/I_G and I_{2D}/I_G ratios, have been presented in (Fig. 4).

The Raman spectroscopy data (Fig. 4) reveals that PAMAM dendrimer functionalization of CNO impacts both disorder (I_D/I_G ratio) and electronic properties (I_{2D}/I_G ratio) in nuanced ways. A statistically significant increase in the I_D/I_G ratio is observed from p-CNO to **CNO-PAMAM 2.0G**, suggesting an increase in defects or disorder introduced by the dendrimer functionalization. On the other hand, no significant change is observed in **CNO-PAMAM 2.0G** and **CNO-PAMAM 2.5G**. There are several contributing factors for which no increase or a relatively lower increase small decrease in the I_D/I_G ratio could be observed. The foremost reason is the degree of functionalization; a higher surface loading is proportional to the increase in the I_D/I_G ratio, as more sp^2 carbon is converted into sp^3. However, these two generations of dendrimers could selectively passivate surface defect sites, which might reduce the Raman spectroscopic signature associated with defects, leading to a lower perceived I_D/I_G ratio. Notwithstanding, as dendrimer generation increases, a pronounced inversely proportional trend of decreasing I_{2D}/I_G ratio is observed in all PAMAM-functionalized samples. This trends suggest alterations in electronic structure and interlayer interactions of the materials [65]—notably, the decrease in the I_{2D}/I_G ratio aligns with a general trend towards thicker layered structures as dendrimer generation increases.

All the materials were characterized by XPS to evaluate the presence, the oxidation state and the surface concentration of the elements contained, and this data is collected in Table 2. The high-resolution C 1*s*, O 1*s*, N 1*s* and S 2*p* spectra for p-CNO and the three CNO-PAMAM hybrids are reported in Fig. 5. The parental p-CNO show no surface oxygen, as the O 1*s* signal is completely absent on them whereas it is present in the three functionalized materials due to the presence of the amide and ester C═O carbonyl groups. For the nitrogen, it is noteworthy that the XPS analysis allows to distinguish two different contributions for the N 1*s* signal: one is due to the tertiary amide and amino groups at about 400 eV present in all the materials, but as the only contribution for **CNO-PAMAM 2.5G**; the second for the terminal $–NH_2$ group at about 402 eV, which is found in **CNO-PAMAM 2.0G** and **CNO-PAMAM 3.0G**. The percentage ratio, obtained by deconvolution of the N 1*s* peak, is in excellent accordance with the theoretical ratio of the different nitrogen atoms (for the 400 eV peak: **CNO-PAMAM 2.0G** 72 % vs 28 %; **CNO-PAMAM 3.0G** 84 % vs 16 %).

Of extreme importance is the presence of the contribution of sulfur, given its critical bridging role in the disulfide-linked CNO-PAMAM *x*G hybrids. Indeed, the sulfur contribution in the XPS affirms the successful coupling of the PAMAM dendron core onto the CNO surface. More specifically, the observed S 2*p* contribution comprises two spin-orbit doublets, indicating the presence of two different species having the two spin-orbit coupling components, namely S $2p_{3/2}$ and S $2p_{1/2}$. The S $2p_{3/2}$ component is centered at about 164 eV, attributable to thioether sulfur bound to a graphitic skeleton [66,67], and the S $2p_{1/2}$ component, centered at about 168.5 eV, occurs due to sulfonic sulfur [68,69]. This finding is analogous to the addition of disulfides to other CNMs, wherein, during functionalization, the sulfur undergoes a partial oxidation to its sulphonic form [51,52]. These results indicate that, in addition to the CNO–S–dendrimer bridge, the dendritic skeletons are also bound to the CNO surface by means of a CNO–SO_2–dendrimer bridge.

Finally, it is worth noting that, in the three materials, the atomic N/S ratio is almost identical for **CNO-PAMAM 2.0G** and **CNO-PAMAM 2.5G**

Table 2
XPS data of CNO-PAMAM *x*G hybrid materials. Binding energies are in square brackets and relative atomic % are italicized.

	C 1*s* *atomic %* [eV]	O 1*s* *atomic %* [eV]	N 1*s* *atomic %* [eV]	S $2p_{3/2}$ *atomic %* [eV]	N/S atomic ratio	N/O atomic ratio
p-CNO	*100.0*	–	–	–	–	–
	284.5	–	–	–		
CNO-PAMAM 2.0G	*87.5*	*5.5*	*6.2*	*0.8*	7.7	1.1
	[284.5] (80 %)	[531.7] (76 %)	[400.0] (72 %)	[163.9] (56 %)		
	[286.2] (15 %)	[533.3] (24 %)	[401.8] (28 %)	[168.2] (44 %)		
	[288.0] (5 %)					
CNO-PAMAM 2.5G(I)	*86.4*	*6.9*	*5.8*	*0.9*	6.3	0.8
	[284.4] (68 %)	[531.8] (64 %)	[400.0] (100 %)	[163.8] (67 %)		
	[285.0] (17 %)	[533.8] (36 %)		[168.6] (33 %)		
	[286.5] (12 %)					
	[288.6] (3 %)					
CNO-PAMAM 3.0G(II)	*84.8*	*5.4*	*9.1*	*0.7*	12.8	1.7
	[284.5] (33 %)	[532.4] (79 %)	[400.7] (84 %)	[164.4] (73 %)		
	[286.0] (53 %)	[533.6] (21 %)	[402.6] (16 %)	[169.0] (27 %)		
	[288.6] (6 %)					
	[290.6] (8 %)					

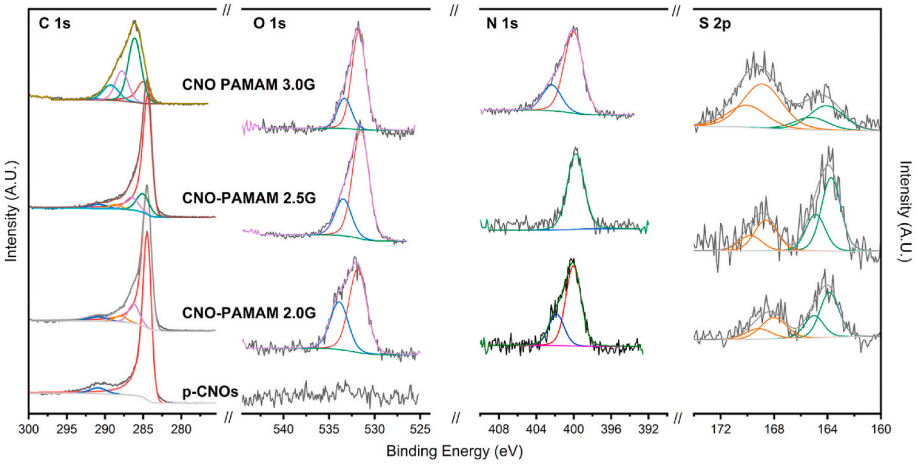

Fig. 5. High-resolution XPS spectra (C 1*s*, O 1*s*, N 1*s*, S 2*p*) of p-CNO and the three CNO-PAMAM *x*G materials.

(I) and almost double for **CNO-PAMAM 3.0G(II)**. Although these values are not exactly the real ratio, they perfectly reflect that **CNO-PAMAM 3.0G(II)** has an N/S ratio almost double that of the other two materials.

HRTEM was used to investigate the morphology of both the p-CNO and **CNO-PAMAM 3.0G(II)** (Fig. S1). TEM images showed that the structure of CNO was unaffected upon chemical modification.

Conversely, their textural properties, determined by N_2 physisorption measurements, showed remarkable differences. The results in terms of total surface area and microporous area are indicated in Table S1 p-CNO shows a surface area of 642 m^2g^{-1}. The micropores of the material (<2 nm), obtained by t-plot analysis, contribute for 123 m^2g^{-1}. Upon functionalization, the microporous structure disappears, and the total surface area of **CNO-PAMAM 3.0G(II)** decreases to 176 m^2g^{-1}. Anyway, the pores size (shown in the inlet of Fig. S2) maintains the same distribution, namely centered at 20 nm.

DLS and ZP are two complementary techniques in the detailed characterization of carbon nanoparticles (CNPs). DLS analyses scattered light to infer the size distribution and aggregation behavior of nano- and microparticles in suspension. On the other hand, ZP reveals the surface charge inherent in these particles, which plays a crucial role in predicting their stability and interaction behavior in colloidal systems [70].

The analysis of these properties in CNPs is of significant interest, given the increasing drive for their use in nanopharmaceuticals and targeted drug delivery systems [31,71,72]. The aqueous solubility dispersion of CNPs remains a significant challenge for their transition into bio-applications, given the propensity for carbon nanoforms to aggregate [73]. To date, this challenge has been addressed through various surface modification approaches [74–76]. Consequently, we are led to an intriguing inquiry: can PAMAM enhance the solubility of CNO in water-based solutions?

DLS and ZP (Fig. 6) analyses of **CNO-PAMAM 2.0G**, **CNO-PAMAM 2.5G(I)** and **CNO-PAMAM 3.0G(II)** were carried out in deionized water at concentrations of 5, 10 and 20 ppm. For each sample, several measurements were taken, which are represented as faint traces in each subplot. From these individual measurements, a representative average curve was calculated and visualized for each material at each concentration. This curve, shown as the thick line, represents the most common particle size in the suspension in DLS studies, and the most common particle surface potential in ZP studies. These DLS results, coupled with the ZP findings, provide crucial insights into the aqueous stability afforded by PAMAM-functionalization on CNO.

ZP results demonstrated optimal values, specifically less than −25 mV when all materials were dispersed at 5 and 10 ppm concentrations. However, a ZP shift towards 0 mV was observed when the materials were dispersed at 20 ppm, indicating a greater propensity towards aggregation at this concentration. This indicates that the stability of CNO-PAMAM nanoparticles in water diminishes at concentrations exceeding 20 ppm.

Of the three generations, **CNO-PAMAM 2.5G(I)** and **CNO-PAMAM 3.0G(II)** demonstrated superior ZP results. The ZP of **CNO-PAMAM 2.0G** was acceptable only at 5 ppm, with a value of approximately −20 ± 2 mV. At concentrations of 10 and 20 ppm, the ZP values for **CNO-PAMAM 2.0G** were not conducive to stability. This instability is corroborated by the DLS findings, which show a significant increase in

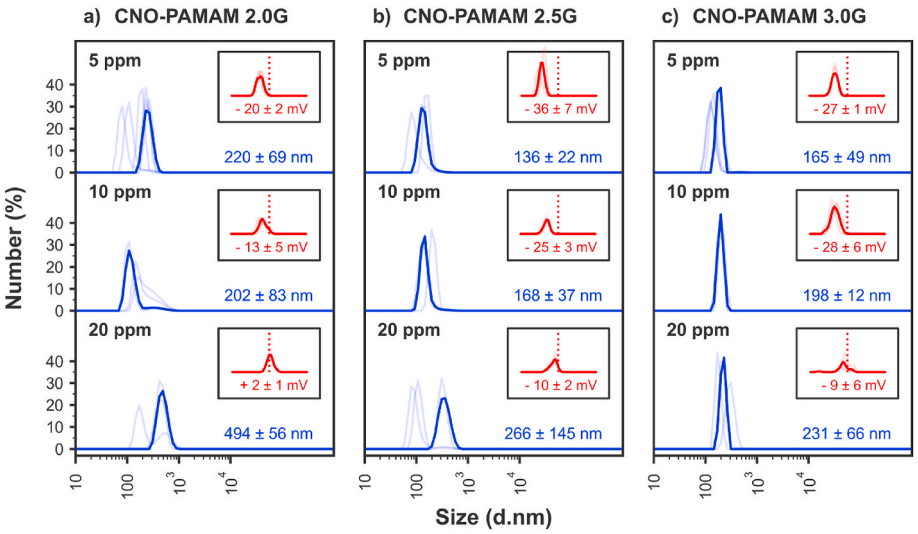

Fig. 6. DLS plots (blue) with ZP inset plots (red) of three generations of CNO-PAMAM *x*G dispersed in deionized water at concentrations of 5, 10 and 20 ppm. The mean ± standard deviation hydrodynamic diameter and ZP values are noted ($n \geq 3$), with individual measurements shown as faint traces.

particle size for **CNO-PAMAM 2.0G** at 20 ppm (494 ± 56 nm), and high deviation between individual measurements at 5 and 10 ppm. Hence, it can be inferred that the 2.0 generation of PAMAM dendrimers is sub-optimal for inferring good aqueous dispersion on CNO.

Notwithstanding, both **CNO-PAMAM 2.5G(I)** and **CNO-PAMAM 3.0G(II)** demonstrated promising performance, maintaining favorable average particle sizes (<200 nm) at 5 and 10 ppm. Notably, **CNO-PAMAM 3.0G(II)** exhibited the most monodispersed distribution, as evidenced by its narrow distribution bands. The standout result was observed for **CNO-PAMAM 3.0G(II)** at 10 ppm, which consistently maintained an excellent distribution size of 198 ± 12 nm and a ZP of −28 ± 6 mV over multiple measurements.

By plotting the DLS results in terms of nanoparticle hydrodynamic diameter as a function of time from the moment the first measurement is taken after sample preparation, we gain further insight into the dispersion stability of the three generations of CNO-PAMAM xG dispersed in deionized water. This time-dependent analysis (Fig. S3) highlights the overall trend of agglomeration of these materials immediately post-sample preparation, with Pearson's *r* value indicating the direction of correlation, supported with an associated *p*-value. The rate of agglomeration is also highlighted, which was computed based on the slope and standard error of the linear regression. Overall, these time-dependent results support the above observations. The best results are observed for **CNO-PAMAM 2.5G** and **CNO-PAMAM 3.0G** when dispersed at 10 ppm; whilst the poorest result is observed in the 20 ppm dispersion of **CNO-PAMAM 2.0G**, which shows a statistically significant (Pearson's $r = 1.00$; $p \leq 0.01$) tendency towards agglomeration, with an interpolated agglomeration rate of 74 ± 1 d nm/min.

Overall, the collective interpretation of these DLS and ZP results offers insights into the influence of PAMAM-functionalization on the aqueous stability of CNO. Given the favorable results demonstrated by **CNO-PAMAM 2.5G(I)** and **CNO-PAMAM 3.0G(II)**, further studies can be envisaged that would contribute to the bio-applications of PAMAM dendrimers in improving CNO dispersibility—namely, given the primary amino tail-end terminations of 3.0G, which are not present in the 2.5G PAMAM dendrimer, it can be speculated that a further improved dispersibility may be attained by lowering the pH of the aqueous dispersions.

To compare the superficial availability of PAMAM amino groups, which can be influenced by the steric hindrance, especially in the case of higher generation dendrimer, we decided to test **CNO-PAMAM 2.0G** and **CNO-PAMAM 3.0G(II)** as possible heterogeneous organocatalysts in the one-pot three-component synthesis in water of some derivative of 2-amino-4*H*-chromene (Scheme 2).

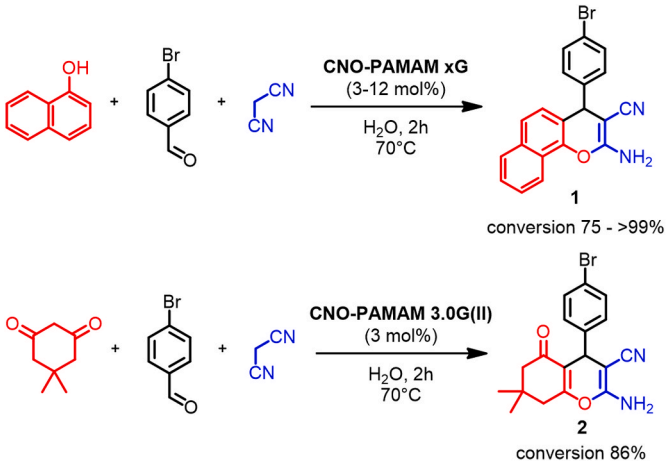

Scheme 2. One-pot synthesis of 2-amino-4*H*-chromene derivatives mediated by CNO-PAMAM *x*G hybrids.

The one-pot synthesis of 2-amino-3-cyano-4-(4-bromophenyl)-4*H*-benzo[*h*]chromene **1** has been selected as the benchmark reaction, and a quick solvent screening prepositioned water as the best reaction media. The hybrids **CNO-PAMAM 2.0G** and **CNO-PAMAM 3.0G(I)** and **(II)** were first tested in 3 mol% content (referred to –NH_2 groups, entries 1–3), being the first the most active with a conversion of 89 % (Table 3,

Table 3
CNO-PAMAM mediated synthesis of 2-amino-4*H*-chromene derivatives **1**–**2**.

Entry	Catalyst	Loading (mol%)	Product	Conversion (%)
1[a]	CNO-PAMAM 2.0G	3	1	89
2[a]	CNO-PAMAM 3.0G(I)	3	1	75
3[a]	CNO-PAMAM 3.0G(II)	3	1	81
4[a]	CNO-PAMAM 3.0G(II)	12	1	>99
5[a]	p-CNO	1.6 mg	–	–
6[a]	Blank test	–	–	–
7[b]	CNO-PAMAM 3.0G(II)	53	2	86

[a] Reaction conditions: 4-bromobenzaldehyde (0.2 mmol), 1-naphthol (0.2 mmol), malononitrile (0.22 mmol), catalyst, water (0.5 mL), 2 h, 70 °C.
[b] Reaction conditions: 4-bromobenzaldehyde (0.25 mmol), dimedone (0.25 mmol), malononitrile (0.3 mmol), catalyst, water (0.5 mL), 12 h, 70 °C.

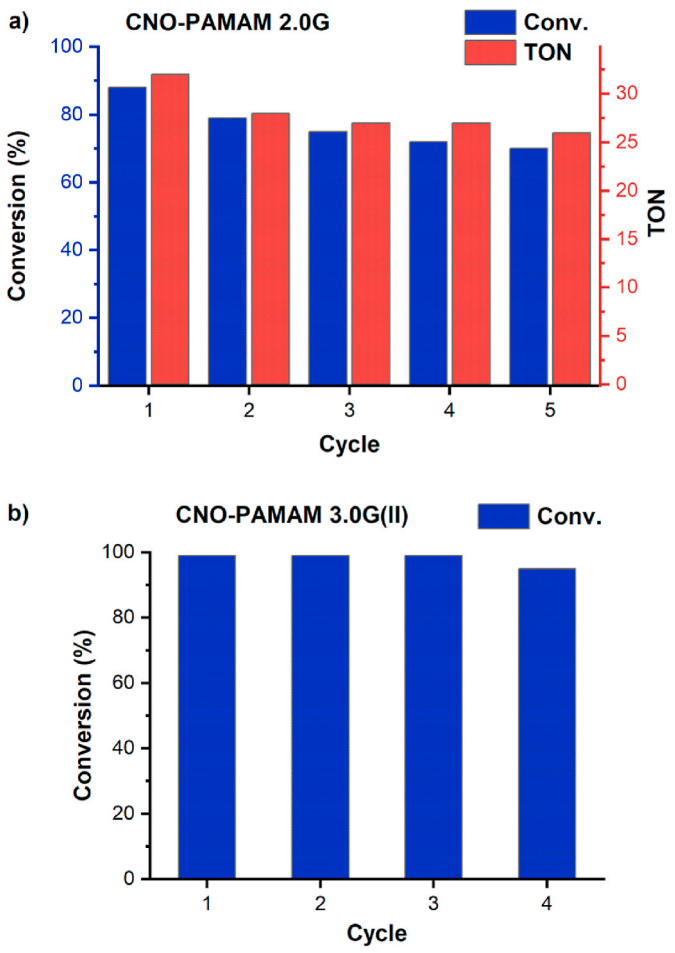

Fig. 7. Recycles with (a) **CNO-PAMAM 2.0G**, (3 mol%), and (b) **CNO-PAMAM 3.0G(II)** (12 mol%).

entry 1). Nevertheless, the higher loading in amino-groups of **CNO-PAMAM 3.0G(II)** (4.21 mmol/g) makes this catalyst more useful since just about one-quarter of the weight is sufficient to guarantee a similar conversion value to the corresponding 4*H*-chromene derivative compared to the case when **CNO-PAMAM 2.0G** (0.94 mmol/g) is used. In addition, a second attempt with 12 mol% of this hybrid gave complete formation of the 4*H*-chromene derivative (Table 3, entry 4).

In addition, further catalytic tests were carried out in the presence of p-CNO (Table 3, entry 5) or without any catalyst (blank test, Table 3, entry 6). In both cases, no trace of 2-amino-3-cyano-4-(4-bromophenyl)-4*H*-benzo[*h*]chromene **1** was detected.

The convenience of applying heterogeneous catalysis relies on the ease of catalyst recovery and its reuse. In this regard, the recyclability of **CNO-PAMAM 2.0G** (3 mol%) and **CNO-PAMAM 3.0G(II)** (12 mol%) was checked for the title reaction (Fig. 7). In the case of **CNO-PAMAM 2.0G**, the conversion of the benzaldehyde into the chromene-derivative gradually diminishes from 89 % to 70 %. Nevertheless, this finding is not associated with loss in activity but with little losses of materials after the recovery (before proceeding with the fourth cycle, the weight of the recovered catalyst was checked, and the amounts of reagents scaled accordingly), given that the turnover number (TON) associated with the actual catalytic loading stays in the 26–28 range between the second and the fifth cycle (Fig. 7). On the other hand, catalyst **CNO-PAMAM 3.0G** yields almost quantitative substrate conversion within 2 h in four consecutive runs (Fig. 7).

Finally, **CNO-PAMAM 3.0G(II)** catalyst successfully converted 4-bromobenzaldehyde to the corresponding 2-amino-4*H*-chromene derivative **2** in 86 % yield when dimedone was used in place of 1-naphthol (Scheme 2 and Table 3, entry 7).

In Scheme S1 a proposed mechanism for the synthesis of 2-amino-4*H*-chromene derivatives catalyzed by CNO-PAMAM hybrids is shown. The reaction starts with the formation of α,β-unsaturated derivative **I** through the Knoevenagel condensation between 4-bromobenzaldehyde and malononitrile in the presence of **CNO-PAMAM 2.0G** or **CNO-PAMAM 3.0G(II)** hybrids. The basic conditions allow for the formation of the enolate ion **II** that performs a Michael addition on the Knoevenagel adduct **I** to obtain intermediate **III** that after a cyclization reaction affords compound **IV**, which tautomerizes to afford the corresponding product **V**.

4. Conclusion

A new easy and atom-economical protocol for the covalent functionalization of carbon nano-onions (CNO) through the radical addition reaction of disulfides has been reported. Three different poly(amidoamine) (PAMAM) dendrimers of increasing generation were successfully bound onto the CNO surface, with corresponding hybrids indicating that reaction time imparts control over the degree of functionalization. These CNO-PAMAM hybrids were extensively characterized using various analytical and spectroscopic techniques.

The TGA was used to establish the degree of functionalization of CNO both in dendron and in amino groups (where present), indicating a loading as high as 4.21 mmol/g for **CNO-PAMAM 3.0G(II)**.

Useful information was obtained from the XPS analysis, which made it possible to establish without a doubt that the dendrimeric skeletons were actually bonded on the surface of the CNO and that this occurs by means of CNO–S–dendrimer and CNO–SO_2–dendrimer bonds, being the sulfur partly oxidized during the radical addition process. In a key result of this study, for the first time it was possible to acquire solid-state CP-MAS ^{13}C NMR spectra of CNO derivatives. The analysis of the DLS and ZP data on the hybrids allowed to establish the dimensions of the aggregates and their stability in aqueous solutions, highlighting the goodness of these in the cases of **CNO-PAMAM 2.5G** and **CNO-PAMAM 3.0G**, which become thus excellent candidates for subsequent studies in the bio-application field.

Regarding their catalytic performance, **CNO-PAMAM 2.0G** and **CNO-PAMAM 3.0G** were found to be good heterogeneous catalysts in three-component one-pot processes for the synthesis of 2-amino-4*H*-chromene derivatives, resulting in easily recoverable and recyclable, with no losses in catalytic activity observed for at least five cycles.

These findings pave the way toward the preparation of other f-CNO with different functional disulfides, for the preparation of more complex CNO-based catalytic systems, and for the preparation of new hybrid systems for drug delivery or with biological activity.

CRediT authorship contribution statement

Alessandro Mercadante: Investigation, Formal analysis, Data curation. **Michal Bartkowski:** Writing – original draft, Investigation, Formal analysis, Data curation. **Vincenzo Campisciano:** Writing – original draft, Supervision, Investigation, Formal analysis, Data curation. **Valeria La Parola:** Writing – original draft, Investigation, Formal analysis, Data curation. **Alberto Spinella:** Writing – original draft, Investigation, Formal analysis, Data curation. **Raul Arenal:** Data curation, Formal analysis. **Michelangelo Gruttadauria:** Writing – original draft, Supervision, Conceptualization. **Silvia Giordani:** Writing – original draft, Supervision, Formal analysis, Data curation. **Francesco Giacalone:** Writing – original draft, Supervision, Methodology, Funding acquisition, Conceptualization.

Declaration of competing interest

The authors declare that they have no known competing financial interests or personal relationships that could have appeared to influence

the work reported in this paper.

Acknowledgements

This research was funded by University of Palermo and the Italian Ministry of Education (PRIN 2017 project no. 2017W8KNZW). The authors thank Prof. S. Agnello and Dr. L. Tranchina (ATeN Center, University of Palermo) for the access to Raman spectroscopy. The authors are also grateful to Dr. M. Scopelliti (ATeN Center, University of Palermo) for the XPS measurements. RA acknowledges funding from the Spanish MICIU (PID2019-104739GB-100/AEI/10.13039/501100011033 and CEX2023-001286-S MICIU/AEI /10.13039/501100011033) as well as from the Gobierno de Aragon (DGA) under project E13-23R. TEM imaging studies have been conducted in the Laboratorio de Microscopias Avanzadas (LMA) at Universidad de Zaragoza. SG acknowledges support from Science Foundation Ireland (22/FFP-A/11067). SG and RA acknowledge support from COST Action CA21126 - Carbon molecular nanostructures in space (NanoSpace), supported by COST (European Cooperation in Science and Technology).

Appendix A. Supplementary data

Supplementary data to this article can be found online at https://doi.org/10.1016/j.carbon.2024.119384.

References

[1] V. Georgakilas, J.A. Perman, J. Tucek, R. Zboril, Broad family of carbon nanoallotropes: classification, chemistry, and applications of fullerenes, carbon dots, nanotubes, graphene, nanodiamonds, and combined superstructures, Chem. Rev. 115 (2015) 4744–4822, https://doi.org/10.1021/cr500304f.
[2] T. Akasaka, F. Wudl, S. Nagase, Chemistry of Nanocarbons, Wiley, Chichester, 2010.
[3] K. Dirian, M.Á. Herranz, G. Katsukis, J. Malig, L. Rodríguez-Pérez, C. Romero-Nieto, V. Strauss, N. Martín, D.M. Guldi, Low dimensional nanocarbons – chemistry and energy/electron transfer reactions, Chem. Sci. 4 (2013) 4335–4353, https://doi.org/10.1039/C3SC51100F.
[4] S.I. Amaral, R. Costa-Almeida, I.C. Gonçalves, F.D. Magalhães, A.M. Pinto, Carbon nanomaterials for phototherapy of cancer and microbial infections, Carbon 190 (2022) 194–244, https://doi.org/10.1016/j.carbon.2021.12.084.
[5] Y. Lin, X. Sun, D.S. Su, G. Centi, S. Perathoner, Catalysis by hybrid sp2/sp3 nanodiamonds and their role in the design of advanced nanocarbon materials, Chem. Soc. Rev. 47 (2018) 8438–8473, https://doi.org/10.1039/C8CS00684A.
[6] Y. Liu, R.L. Vander Wal, V.N. Khabashesku, Functionalization of carbon nano-onions by direct fluorination, Chem. Mater. 19 (2007) 778–786, https://doi.org/10.1021/cm062177j.
[7] J. Bartelmess, S. Giordani, Carbon nano-onions (multi-layer fullerenes): chemistry and applications, Beilstein J. Nanotechnol. 5 (2014) 1980–1998, https://doi.org/10.3762/bjnano.5.207.
[8] A. Palkar, A. Kumbhar, A.J. Athans, L. Echegoyen, Pyridyl-functionalized and water-soluble carbon nano onions: first supramolecular complexes of carbon nano onions, Chem. Mater. 20 (2008) 1685–1687, https://doi.org/10.1021/cm7035508.
[9] A.S. Rettenbacher, B. Elliott, J.S. Hudson, A. Amirkhanian, L. Echegoyen, Preparation and functionalization of multilayer fullerenes (carbon nano-onions), Chem. Eur J. 12 (2006) 376–387, https://doi.org/10.1002/chem.200500517.
[10] L. Zhou, C. Gao, D. Zhu, W. Xu, F.F. Chen, A. Palkar, L. Echegoyen, E.S.-W. Kong, Facile functionalization of multilayer fullerenes (carbon nano-onions) by nitrene chemistry and “grafting from” strategy, Chem. Eur J. 15 (2009) 1389–1396, https://doi.org/10.1002/chem.200801642.
[11] V. Georgakilas, D.M. Guldi, R. Signorini, R. Bozio, M. Prato, Organic functionalization and optical properties of carbon onions, J. Am. Chem. Soc. 125 (2003) 14268–14269, https://doi.org/10.1021/ja0342805.
[12] K. Flavin, M.N. Chaur, L. Echegoyen, S. Giordani, Functionalization of multilayer fullerenes (carbon nano-onions) using diazonium compounds and “click” chemistry, Org. Lett. 12 (2010) 840–843, https://doi.org/10.1021/ol902939f.
[13] M. Frasconi, R. Marotta, L. Markey, K. Flavin, V. Spampinato, G. Ceccone, L. Echegoyen, E.M. Scanlan, S. Giordani, Multi-functionalized carbon nano-onions as imaging probes for cancer cells, Chem. Eur J. 21 (2015) 19071–19080, https://doi.org/10.1002/chem.201503166.
[14] A. Molina-Ontoria, M.N. Chaur, M.E. Plonska-Brzezinska, L. Echegoyen, Preparation and characterization of soluble carbon nano-onions by covalent functionalization, employing a Na–K alloy, Chem. Commun. 49 (2013) 2406–2408, https://doi.org/10.1039/C3CC39077B.
[15] M.E. Pérez-Ojeda, E. Castro, C. Kröckel, M.A. Lucherelli, U. Ludacka, J. Kotakoski, K. Werbach, H. Peterlik, M. Melle-Franco, J.C. Chacón-Torres, F. Hauke, L. Echegoyen, A. Hirsch, G. Abellán, Carbon nano-onions: potassium intercalation and reductive covalent functionalization, J. Am. Chem. Soc. 143 (2021) 18997–19007, https://doi.org/10.1021/jacs.1c07604.
[16] V. Dhand, M. Yadav, S.H. Kim, K.Y. Rhee, A comprehensive review on the prospects of multi-functional carbon nano onions as an effective, high-performance energy storage material, Carbon 175 (2021) 534–575, https://doi.org/10.1016/j.carbon.2020.12.083.
[17] M. Zeiger, N. Jäckel, V.N. Mochalin, V. Presser, Review: carbon onions for electrochemical energy storage, J. Mater. Chem. A 4 (2016) 3172–3196, https://doi.org/10.1039/C5TA08295A.
[18] Y. Liu, D.Y. Kim, Ultraviolet and blue emitting graphene quantum dots synthesized from carbon nano-onions and their comparison for metal ion sensing, Chem. Commun. 51 (2015) 4176–4179, https://doi.org/10.1039/C4CC07618D.
[19] F.R. Baptista, S.A. Belhout, S. Giordani, S.J. Quinn, Recent developments in carbon nanomaterial sensors, Chem. Soc. Rev. 44 (2015) 4433–4453, https://doi.org/10.1039/C4CS00379A.
[20] V. Singh, Natural source derived carbon nano-onions as electrode material for sensing applications, Diam. Relat. Mater. 87 (2018) 202–207, https://doi.org/10.1016/j.diamond.2018.06.007.
[21] D. Pech, M. Brunet, H. Durou, P. Huang, V. Mochalin, Y. Gogotsi, P.-L. Taberna, P. Simon, Ultrahigh-power micrometre-sized supercapacitors based on onion-like carbon, Nat. Nanotechnol. 5 (2010) 651–654, https://doi.org/10.1038/nnano.2010.162.
[22] Y. Gao, Y.S. Zhou, M. Qian, X.N. He, J. Redepenning, P. Goodman, H.M. Li, L. Jiang, Y.F. Lu, Chemical activation of carbon nano-onions for high-rate supercapacitor electrodes, Carbon 51 (2013) 52–58, https://doi.org/10.1016/j.carbon.2012.08.009.
[23] B. Xu, X. Yang, X. Wang, J. Guo, X. Liu, A novel catalyst support for DMFC: onion-like fullerenes, J. Power Sources 162 (2006) 160–164, https://doi.org/10.1016/j.jpowsour.2006.06.063.
[24] S. Porada, L. Borchardt, M. Oschatz, M. Bryjak, J.S. Atchison, K.J. Keesman, S. Kaskel, P.M. Biesheuvel, V. Presser, Direct prediction of the desalination performance of porous carbon electrodes for capacitive deionization, Energy Environ. Sci. 6 (2013) 3700–3712, https://doi.org/10.1039/C3EE42209G.
[25] M.E. Plonska-Brzezinska, Carbon nano-onions: a review of recent progress in synthesis and applications, Chem. Nano Mat. 5 (2019) 568–580, https://doi.org/10.1002/cnma.201800583.
[26] S. Giordani, A. Camisasca, V. Maffeis, Carbon nano-onions: a valuable class of carbon nanomaterials in biomedicine, Curr. Med. Chem. 26 (2019) 6915–6929, https://doi.org/10.2174/0929867326666181126113957.
[27] J. Bartelmess, E. De Luca, A. Signorelli, M. Baldrighi, M. Becce, R. Brescia, V. Nardone, E. Parisini, L. Echegoyen, P.P. Pompa, S. Giordani, Boron dipyrromethene (BODIPY) functionalized carbon nano-onions for high resolution cellular imaging, Nanoscale 6 (2014) 13761–13769, https://doi.org/10.1039/C4NR04533E.
[28] M. Frasconi, V. Maffeis, J. Bartelmess, L. Echegoyen, S. Giordani, Highly surface functionalized carbon nano-onions for bright light bioimaging, Methods Appl. Fluoresc. 3 (2015) 044005, https://doi.org/10.1088/2050-6120/3/4/044005.
[29] M. d’Amora, V. Maffeis, R. Brescia, D. Barnes, E. Scanlan, S. Giordani, Carbon nano-onions as non-cytotoxic carriers for cellular uptake of glycopeptides and proteins, Nanomaterials 9 (2019) 1069, https://doi.org/10.3390/nano9081069.
[30] M. Bartkowski, V. Bincoletto, I.C. Salaroglio, G. Ceccone, R. Arenal, S. Nervo, B. Rolando, C. Riganti, S. Arpicco, S. Giordani, Enhancing pancreatic ductal adenocarcinoma (PDAC) therapy with targeted carbon nano-onion (CNO)-mediated delivery of gemcitabine (GEM)-derived prodrugs, J. Colloid Interface Sci. 659 (2024) 339–354, https://doi.org/10.1016/j.jcis.2023.12.166.
[31] M. Bartkowski, S. Giordani, Carbon nano-onions as potential nanocarriers for drug delivery, Dalton Trans. 50 (2021) 2300–2309, https://doi.org/10.1039/D0DT04093B.
[32] N. Keller, N.I. Maksimova, V.V. Roddatis, M. Schur, G. Mestl, Y.V. Butenko, V. L. Kuznetsov, R. Schlögl, The catalytic use of onion-like carbon materials for styrene synthesis by oxidative dehydrogenation of ethylbenzene, Angew. Chem. Int. Ed. 41 (2002) 1885–1888, https://doi.org/10.1002/1521-3773(20020603)41:11<1885::AID-ANIE1885>3.0.CO;2-5.
[33] D. Su, N.I. Maksimova, G. Mestl, V.L. Kuznetsov, V. Keller, R. Schlögl, N. Keller, Oxidative dehydrogenation of ethylbenzene to styrene over ultra-dispersed diamond and onion-like carbon, Carbon 45 (2007) 2145–2151, https://doi.org/10.1016/j.carbon.2007.07.005.
[34] V. Maffeis, R.O. McCourt, R. Petracca, O. Laethem, A. Camisasca, P.E. Colavita, S. Giordani, E.M. Scanlan, Photocatalytic initiation of radical thiol–ene reactions using carbon-Bi2O3 nanocomposites, ACS Appl. Nano Mater. 1 (2018) 4120–4126, https://doi.org/10.1021/acsanm.8b00870.
[35] S.F. Mohammadi Metkazini, Z. Khorsandi, A. Heydari, R.S. Varma, Sustainable visible light-driven heck and suzuki reactions using NiCu nanoparticles adorned on carbon nano-onions, ACS Sustain. Chem. Eng. 9 (2021) 14061–14069, https://doi.org/10.1021/acssuschemeng.1c03499.
[36] X. Yan, P. Duan, F. Zhang, H. Li, H. Zhang, M. Zhao, X. Zhang, B. Xu, S. J. Pennycook, J. Guo, Stable single-atom platinum catalyst trapped in carbon onion graphitic shells for improved chemoselective hydrogenation of nitroarenes, Carbon 143 (2019) 378–384, https://doi.org/10.1016/j.carbon.2018.11.021.
[37] C.G. Renda, L.A. Goulart, C.H.M. Fernandes, L.H. Mascaro, J.M. de Aquino, R. Bertholdo, Novel onion-like carbon structures modified with iron oxide as photocatalysts for the degradation of persistent pollutants, J. Environ. Chem. Eng. 9 (2021) 104934, https://doi.org/10.1016/j.jece.2020.104934.
[38] K. Chatterjee, M. Ashokkumar, H. Gullapalli, Y. Gong, R. Vajtai, P. Thanikaivelan, P.M. Ajayan, Nitrogen-rich carbon nano-onions for oxygen reduction reaction, Carbon 130 (2018) 645–651, https://doi.org/10.1016/j.carbon.2018.01.052.

[39] W. Liu, B. Chen, X. Duan, K.-H. Wu, W. Qi, X. Guo, B. Zhang, D. Su, Molybdenum carbide modified nanocarbon catalysts for alkane dehydrogenation reactions, ACS Catal. 7 (2017) 5820–5827, https://doi.org/10.1021/acscatal.7b01905.
[40] W. Liu, W. Qi, X. Guo, D. Su, Heteropoly acid/nitrogen functionalized onion-like carbon hybrid catalyst for ester hydrolysis reactions, Chem. Asian J. 11 (2016) 491–497, https://doi.org/10.1002/asia.201500944.
[41] E. Regulska, P. Olejnik, H. Zubyk, J. Czyrko-Horczak, M.N. Chaur, M. Tomczykowa, O. Butsyk, K. Brzezinski, L. Echegoyen, M.E. Plonska-Brzezinska, Nanostructural catalyst: metallophthalocyanine and carbon nano-onion with enhanced visible-light photocatalytic activity towards organic pollutants, RSC Adv. 10 (2020) 10910–10920, https://doi.org/10.1039/D0RA00896F.
[42] G.P. Ellis, Chromanones Chromenes, Chromones, The Series "The Chemistry of Heterocyclic Compounds, 31, John Wiley & Sons, 1977.
[43] M.T. Flavin, J.D. Rizzo, A. Khilevich, A. Kucherenko, A.K. Sheinkman, V. Vilaychack, L. Lin, W. Chen, E.M. Greenwood, T. Pengsuparp, J.M. Pezzuto, S. H. Hughes, T.M. Flavin, M. Cibulski, W.A. Boulanger, R.L. Shone, Z.-Q. Xu, Synthesis, chromatographic resolution, and anti-human immunodeficiency virus activity of (±)-Calanolide A and its enantiomers, J. Med. Chem. 39 (1996) 1303–1313, https://doi.org/10.1021/jm950797i.
[44] P.W. Smith, S.L. Sollis, P.D. Howes, P.C. Cherry, I.D. Starkey, K.N. Cobley, H. Weston, J. Scicinski, A. Merritt, A. Whittington, P. Wyatt, N. Taylor, D. Green, R. Bethell, S. Madar, R.J. Fenton, P.J. Morley, T. Pateman, A. Beresford, Dihydropyrancarboxamides related to zanamivir: a new series of inhibitors of influenza virus sialidases. 1. Discovery, synthesis, biological activity, and Structure−Activity relationships of 4-guanidino- and 4-amino-4H-pyran-6-carboxamides, J. Med. Chem. 41 (1998) 787–797, https://doi.org/10.1021/jm970374b.
[45] C. Brühlmann, F. Ooms, P.-A. Carrupt, B. Testa, M. Catto, F. Leonetti, C. Altomare, A. Carotti, Coumarins derivatives as dual inhibitors of acetylcholinesterase and monoamine oxidase, J. Med. Chem. 44 (2001) 3195–3198, https://doi.org/10.1021/jm010894d.
[46] H.K. Keerthy, M. Garg, C.D. Mohan, V. Madan, D. Kanojia, R. Shobith, S. Nanjundaswamy, D.J. Mason, A. Bender, Basappa, K.S. Rangappa, H.P. Koeffler, Synthesis and characterization of novel 2-amino-chromene-nitriles that target bcl-2 in acute myeloid leukemia cell lines, PLoS One 9 (2014) e107118, https://doi.org/10.1371/journal.pone.0107118.
[47] D.A. Tomalia, B. Huang, D.R. Swanson, H.M. Brothers, J.W. Klimash, Structure control within poly(amidoamine) dendrimers: size, shape and regio-chemical mimicry of globular proteins, Tetrahedron 59 (2003) 3799–3813, https://doi.org/10.1016/S0040-4020(03)00430-7.
[48] M.M. Hashemi, H. Ghafuri, Z. Karimi-Jaberi, N-Chlorosuccinimide: a simple and efficient reagent for the preparation of symmetrical disulfides, J. Sulphur Chem. 27 (2006) 165–167, https://doi.org/10.1080/17449200600572506.
[49] D.A. Shirley, High-resolution X-ray photoemission spectrum of the valence bands of gold, Phys. Rev. B 5 (1972) 4709–4714, https://doi.org/10.1103/PhysRevB.5.4709.
[50] S. Giordani, Methods for the preparation of carbon nano-onions, WO/2018/116240. https://patentscope.wipo.int/search/en/detail.jsf?docId=WO2018116240, 2018.
[51] Z. Syrgiannis, V. La Parola, C. Hadad, M. Lucío, E. Vázquez, F. Giacalone, M. Prato, An atom-economical approach to functionalized single-walled carbon nanotubes: reaction with disulfides, Angew. Chem. Int. Ed. 52 (2013) 6480–6483, https://doi.org/10.1002/anie.201301617.
[52] Z. Syrgiannis, A. Bonasera, E. Tenori, V. La Parola, C. Hadad, M. Gruttadauria, F. Giacalone, M. Prato, Chemical modification of carbon nanomaterials (SWCNTs, DWCNTs, MWCNTs and SWCNHs) with diphenyl dichalcogenides, Nanoscale 7 (2015) 6007–6013, https://doi.org/10.1039/C4NR07196D.
[53] F. Giacalone, V. Campisciano, C. Calabrese, V. La Parola, Z. Syrgiannis, M. Prato, M. Gruttadauria, Single-Walled carbon nanotube–polyamidoamine dendrimer hybrids for heterogeneous catalysis, ACS Nano 10 (2016) 4627–4636, https://doi.org/10.1021/acsnano.6b00936.
[54] R. Esfand, D.A. Tomalia, Poly(amidoamine) (PAMAM) dendrimers: from biomimicry to drug delivery and biomedical applications, Drug Discov. Today 6 (2001) 427–436, https://doi.org/10.1016/S1359-6446(01)01757-3.
[55] S. Svenson, Dendrimers as versatile platform in drug delivery applications, Eur. J. Pharm. Biopharm. 71 (2009) 445–462, https://doi.org/10.1016/j.ejpb.2008.09.023.
[56] B.K. Nanjwade, H.M. Bechra, G.K. Derkar, F.V. Manvi, V.K. Nanjwade, Dendrimers: emerging polymers for drug-delivery systems, Eur. J. Pharmaceut. Sci. 38 (2009) 185–196, https://doi.org/10.1016/j.ejps.2009.07.008.
[57] P. Kesharwani, K. Jain, N.K. Jain, Dendrimer as nanocarrier for drug delivery, Prog. Polym. Sci. 39 (2014) 268–307, https://doi.org/10.1016/j.progpolymsci.2013.07.005.
[58] S. Svenson, D.A. Tomalia, Dendrimers in biomedical applications—reflections on the field, Adv. Drug Deliv. Rev. 57 (2005) 2106–2129, https://doi.org/10.1016/j.addr.2005.09.018.
[59] S. Svenson, D.A. Tomalia, Dendrimers in biomedical applications—reflections on the field, Adv. Drug Deliv. Rev. 64 (2012) 102–115, https://doi.org/10.1016/j.addr.2012.09.030.
[60] H. Yang, W.J. Kao, Dendrimers for pharmaceutical and biomedical applications, J. Biomater. Sci. Polym. Ed. 17 (2006) 3–19, https://doi.org/10.1163/156856206774879171.
[61] B. Iskin, G. Yilmaz, Y. Yagci, Mono-addition synthesis of polystyrene–fullerene (C60) conjugates by thiol–ene chemistry, Chem. Eur J. 18 (2012) 10254–10257, https://doi.org/10.1002/chem.201200534.
[62] N.D. Luong, L.H. Sinh, L.-S. Johansson, J. Campell, J. Seppälä, Functional graphene by thiol-ene click chemistry, Chem. Eur J. 21 (2015) 3183–3186, https://doi.org/10.1002/chem.201405734.
[63] X.H. Yang, J.W. Guo, S. Yang, Y. Hou, B. Zhang, H.G. Yang, A free radical assisted strategy for preparing ultra-small Pt decorated CNTs as a highly efficient counter electrode for dye-sensitized solar cells, J. Mater. Chem. A 2 (2014) 614–619, https://doi.org/10.1039/C3TA13986G.
[64] A. Palkar, F. Melin, C.M. Cardona, B. Elliott, A.K. Naskar, D.D. Edie, A. Kumbhar, L. Echegoyen, Reactivity differences between carbon nano onions (CNOs) prepared by different methods, Chem. Asian J. 2 (2007) 625–633, https://doi.org/10.1002/asia.200600426.
[65] D.W. Li, Y.S. Zhou, X. Huang, L. Jiang, J.F. Silvain, Y.F. Lu, In situ imaging and control of layer-by-layer femtosecond laser thinning of graphene, Nanoscale 7 (2015) 3651–3659, https://doi.org/10.1039/C4NR07078J.
[66] J. Chattopadhyay, S. Chakraborty, A. Mukherjee, R. Wang, P.S. Engel, W.E. Billups, SET mechanism in the functionalization of single-walled carbon nanotubes, J. Phys. Chem. C 111 (2007) 17928–17932, https://doi.org/10.1021/jp071746n.
[67] N. Takako, O. Tsuguyori, I. Masatou, T. Akihiro, K. Yoshinori, Sidewall modification of single-walled carbon nanotubes with sulfur-containing functionalities and gold nanoparticle attachment, Chem. Lett. 35 (2006) 742–743, https://doi.org/10.1246/cl.2006.742.
[68] F. Iacona, G. Marletta, XPS study of radiation-induced modification of poly(butene-1-sulfone): dependence on the energy deposition mechanism, Nucl. Instrum. Methods Phys. Res. B . 166–167 (2000) 676–681, https://doi.org/10.1016/S0168-583X(99)01186-6.
[69] C. Médard, M. Morin, Chemisorption of aromatic thiols onto a glassy carbon surface, J. Electroanal. Chem. 632 (2009) 120–126, https://doi.org/10.1016/j.jelechem.2009.04.005.
[70] S. Bhattacharjee, DLS and zeta potential – what they are and what they are not? J. Contr. Release 235 (2016) 337–351, https://doi.org/10.1016/j.jconrel.2016.06.017.
[71] D. Peer, J.M. Karp, S. Hong, O.C. Farokhzad, R. Margalit, R. Langer, Nanocarriers as an emerging platform for cancer therapy, Nat. Nanotechnol. 2 (2007) 751–760, https://doi.org/10.1038/nnano.2007.387.
[72] M.J. Mitchell, M.M. Billingsley, R.M. Haley, M.E. Wechsler, N.A. Peppas, R. Langer, Engineering precision nanoparticles for drug delivery, Nat. Rev. Drug Discov. 20 (2021) 101–124, https://doi.org/10.1038/s41573-020-0090-8.
[73] J.C. Zuaznabar-Gardona, A. Fragoso, Determination of the Hansen solubility parameters of carbon nano-onions and prediction of their dispersibility in organic solvents, J. Mol. Liq. 294 (2019) 111646, https://doi.org/10.1016/j.molliq.2019.111646.
[74] M. d'Amora, A. Camisasca, A. Boarino, S. Arpicco, S. Giordani, Supramolecular functionalization of carbon nano-onions with hyaluronic acid-phospholipid conjugates for selective targeting of cancer cells, Colloids Surf., B 188 (2020) 110779, https://doi.org/10.1016/j.colsurfb.2020.110779.
[75] M.A. Lucherelli, L.M.S. Stiegler, F. Steiger, E.H. Åhlgren, J. Requena-Ramírez, E. Castro, L. Echegoyen, A. Hirsch, W. Peukert, J. Kotakoski, J. Walter, M.E. Pérez-Ojeda, G. Abellán, Carbon nano-onions: individualization and enhanced water dispersibility, Carbon 218 (2024) 118760, https://doi.org/10.1016/j.carbon.2023.118760.
[76] M.E. Plonska-Brzezinska, A. Lapinski, A.Z. Wilczewska, A.T. Dubis, A. Villalta-Cerdas, K. Winkler, L. Echegoyen, The synthesis and characterization of carbon nano-onions produced by solution ozonolysis, Carbon 49 (2011) 5079–5089, https://doi.org/10.1016/j.carbon.2011.07.027.